AFRL-AFOSR-CL-TR-2015-0001

STUDY OF HV DIELECTRICS FOR HIGH FREQUENCY OPERATION **IN LINEAR & NONLINEAR TRANSMISSION LINES & SIMULATION & DEVELOPMENT OF HYBRID NONLINEAR LINES FOR RF GENERATION**

Jose Rossi
FUNCATE - FUNDACACAO DE CIENCIAS

08/27/2015
Final Report

Air Force Research Laboratory
AF Office Of Scientific Research (AFOSR)/ IOS
Arlington, Virginia 22203
Air Force Materiel Command

AFOSR Final Performance Report

Study of HV Dielectrics for High Frequency Operation in Linear and Nonlinear Transmission Lines and Simulation and Development of Hybrid Nonlinear Lines for RF Generation

Contract Number: FA9550-13-1-0132

Start Date: 1 March 2013

Program Manager: Mr. James Fillerup
AFOSR/IO
875 North Randolf Street
Suite 325, Room 3112
Arlington VA, 22203
Principal Investigator
Office: +1 703 588-8316
E-mail: james.fillerup@us.af.mil

Principal Investigator: Dr. Jose O. Rossi
National Institute for Space Research (INPE)
Associated Plasma Laboratory
1758 Astronautas Ave.
Sao Jose dos Campos, SP, Brazil, 12227-010
Office: + 55 (12) 3208 6695
E-mail: rossi@plasma.inpe.br

REPORT DOCUMENTATION PAGE

Form Approved
OMB No. 0704-0188

1. REPORT DATE *(DD-MM-YYYY)*	**2. REPORT TYPE**	**3. DATES COVERED** *(From - To)*
August 2015	Final Performance Report	1 March 2013- 31 Aug. 2014

4. TITLE AND SUBTITLE
Study of HV Dielectrics for High Freq. Operation in Linear & Nonlinear Transmission Lines & Development and Simulation of Hvbrid NonLinear Lines for RF Generation

5a. CONTRACT NUMBER
FA9950-13-1-0132

5b. GRANT NUMBER

5c. PROGRAM ELEMENT NUMBER

6. AUTHOR(S)
Jose O. Rossi

5d. PROJECT NUMBER

5e. TASK NUMBER

5f. WORK UNIT NUMBER

7. PERFORMING ORGANIZATION NAME(S) AND ADDRESS(ES)

National Institute for Space
Research –INPE
1758 Astronautas Ave.,
12227010 SJ Campos SP Brazil

8. PERFORMING ORGANIZATION REPORT NUMBER

9. SPONSORING / MONITORING AGENCY NAME(S) AND ADDRESS(ES)

AFOSR/IO
875 North Randolf St.
Arlington, VA, 22203

10. SPONSOR/MONITOR'S ACRONYM(S)
AFOSR

11. SPONSOR/MONITOR'S REPORT NUMBER(S)

12. DISTRIBUTION / AVAILABILITY STATEMENT

DISTRIBUTION A

13. SUPPLEMENTARY NOTES

14. ABSTRACT

The objectives of this work is to describe the research on lumped capacitive nonlinear transmission lines (NLTLs) developed during period 2013-2014. As lumped capacitive NLTLs employ nonlinear dielectric mediums, we have characterized ceramic dielectrics (lead-zirconium and barium titanates, PZT and BT, respectively) in order to address RF soliton generation using these lines. Other issue studied was the investigation of the NLTL principle operation using a low voltage line built with varying capacitance diodes, called varactors, as these components show higher nonlinearity than commercial ceramic capacitors. To assess the performance of BT and PZT dielectrics we have built and tested HV NLTLs. In this case, the main results obtained and their implications on the design of capacitive NLTL operation at high frequencies are also discussed.

15. SUBJECT TERM

16. SECURITY CLASSIFICATION OF:			**17. LIMITATION OF ABSTRACT**	**18. NUMBER OF PAGES**	**19a. NAME OF RESPONSIBLE PERSON**
a. REPORT	**b. ABSTRACT**	**c. THIS PAGE**			**19b. TELEPHONE NUMBER** *(include area code)*
					Jose O. Rossi 55 12 3208 6695

Standard Form 298 (Rev. 8-98)
Prescribed by ANSI Std. Z39.18

1. Status of effort

The ferroelectric ceramics have a nonlinear behavior arising from the variation of the permittivity with voltage, which is a primordial requirement for microwave soliton generation in nonlinear transmission lines (NLTL). Described by a squared hyperbolic secant function, solitons are oscillations generated in lumped NLTLs because dielectric permittivity varies with the amplitude of the applied input pulse [1-3]. These oscillations can be used as microwave signals. In principle NLTLs could provide sub-microwave peak power of tens of megawatts at a certain pulse repetition rate (0.1 – 1 kHz) with dielectric requirements of high voltage breakdown strength (BD-tens of kV/cm) and low loss tangent (< 1%). As shown in [4], [5], the capacitors based on PZT (lead-zirconate-titanate) and BT dielectrics have dielectric BD strength of the order of 50 kV/cm and 100 kV/cm, respectively. Nevertheless, the suppliers do not furnish the loss tangent of these components at sub-GHz frequencies. Other dielectric investigated for applying in high power NLTLs is a piezoelectric ceramic normally used in sensors and transducers in industrial applications, called as Lead-Zirconium-Titanate (PZT). For reduced dielectric losses, PZT is acquired normally de-poled. The acquired PZT material (type 4) was characterized in broadband frequency range, from 0.01 GHz to 1 GHz, using a vector network analyzer (VNA) [6], [7]. To assess nonlinearity property of the dielectrics (BT and PZTs), the materials were characterized as a function of the DC voltage applied and frequency. The complex dielectric constant of materials is calculated by the reflection coefficient (S_{11}) measured using a vector network analyzer (VNA).

Other investigation carried out was the principle of operation of NLTLs. A square pulse injected into the NLTL input is modified by the dispersive and nonlinear effects of the line, modulated and broken up into a group of solitons (oscillating pulses) which are used to feed an RF load through an antenna matched to the output of the line. In low-voltage NLTLs, varactor diodes are used as nonlinear medium since their diode junction capacitance varies with the inverse of the applied reverse voltage [8], [9]. In this report, the experimental results of a varactor diode NLTL built with 30 sections are presented. Besides, Spice simulation provides an excellent way of studying the NLTL principle operation by comparing them with the experimental results obtained. The FFTs of the simulated and experimental output voltage pulsed are also used to investigate the frequency spectrum of the output oscillations obtained.

Finally, in this report, it is described the implementation of a high voltage nonlinear capacitive line (NLCL) using commercial BT and PZT ceramic capacitors. Corresponding NLCL Spice simulation is provided for comparison with experimental results. Depending on the nonlinearity properties of the capacitor dielectric, input pulse rise time, output pulse sharpening and or RF soliton generation can be obtained as described in this report. Some conclusions on the material properties of the dielectrics tested and their effect on soliton RF generation will be discussed in this report too.

2. Dielectric Characterization

In capacitive NLTLs, BT dielectric has been the mostly used so far. However, the dielectric losses of BT have prevented from achieving RF generation above several hundreds of megahertz (200 MHz) with good voltage modulation depth (VMD) of oscillations as pointed out elsewhere [10], [11]. Therefore, this section gives a comparison of the electrical properties between the new proposed dielectric for this application, the PZT, and the well-known BT, considering the material losses, breakdown (BD) strength, nonlinearity and frequency response. For these tests, we used circular PZT samples de-poled by manufacturer (type 4 and type 8) of 20/25 mm diameter, respectively, with thickness of 2 mm and based-BT high-voltage commercial ceramic capacitors of 10 nF/ 2 kV, 1 nF/ 2 kV and 0.47 nF/3 kV.

2.1. Dielectric Losses

For the dielectric loss measurement in a low frequency range, an HP 4285A/ 30 MHz RLC impedance meter was used to measure the dissipation factor of the material (loss tangent) as function of the frequency. Fig. 1 shows the loss tangent measurements for PZT and BT-based ceramic capacitors in a frequency range up to 2 MHz, below the resonant frequency of the both dielectrics. As seen in Fig. 1, PZTs have better performance than BT-based dielectrics in this frequency range because of the PZT lower loss tangent. The reason is that PZT dielectric resistance, namely R_D, is significantly higher in this frequency range as loss tangent in this case is equal to $1/(2\pi f \times R_D \times C)$, neglecting ohmic contact resistances as well as the capacitor charging leakage resistance [12].

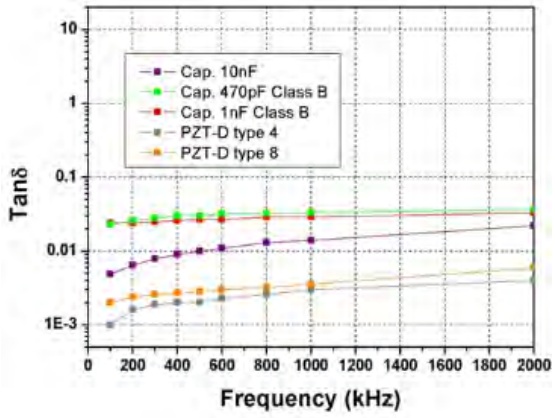

Fig. 1. Loss tangent comparison shown between PZTs and BT-based ceramic capacitors.

The lower dissipation factor observed for de-poled PZTs (at least at lower frequencies) is also confirmed through P×E polarization measurements using 60 Hz alternating fields provided by the well-known Sawyer-Tower Circuit [13] and the x-y mode of a digital scope. The bigger area inside the P×E curve means higher losses. For instance, the P×E curve measured of capacitor of 1 nF/2 kV shows higher losses than that of de-poled type 8 PZT as shown in Fig. 2. The scope x and y scales are multiplied by 1000 because of the HV probes used in the measurements. From the Sawyer-Tower circuit parameters and using dimensions of the dielectrics under tests in Fig. 2 obtains maximum polarization densities of about 4 μC/cm2 and 81 μC/cm2, respectively for PZT and 1nF capacitor, at corresponding maximum electric fields of the order of 5.0 kV/cm and 22.0 kV/cm. In the case of capacitor, the polarization density is higher because of its dielectric with smaller area (ϕ=5.6 mm) submitted to an increased electric field due to the thinner dielectric thickness of 0.68 mm [12].

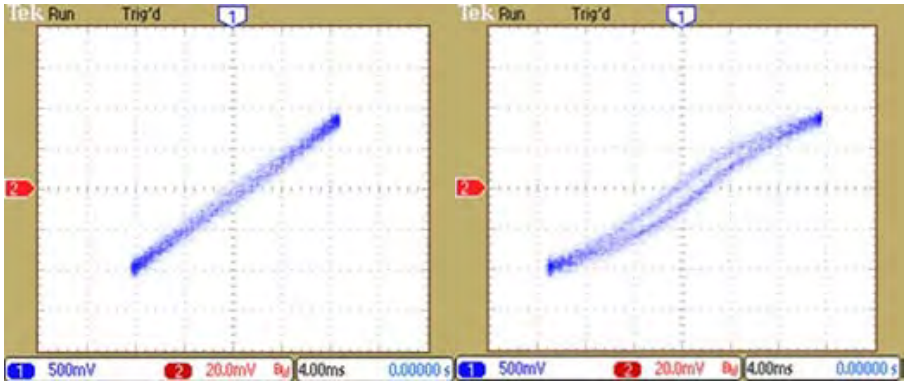

(a) (b)

Fig. 2. P×E loop measured on the scope screen for PZT type 8 (left) and 1nF capacitor (right): CH1–x scale: 1.0 kV/div and CH2- y scale: 20.0 V/div.

2.2. Breakdown

For the HV BD tests, we used an LC oscillatory half sine wave discharge circuit [14]. This circuit is capable of generating a differential voltage across the dielectric under test. The Weibull (WB) statistics were used for 10 samples of each device tested (PZT-4 and ceramic capacitors of 0.47 nF/ 3 kV). As described elsewhere [12], using this method gives an average BD strength of about 43.5 kV/cm for type 4 PZT with a standard deviation of ± 3.6 kV/cm. Similarly, an average BD strength of the order of 86.9 kV/cm is obtained for the ceramic capacitor of 0.47 nF/3 kV with a standard deviation of ± 8.1 kV/cm. By comparing with BT-based capacitors, these results show that PZTs have approximately half the pulsed BD strength of ceramic capacitors. Although, BD statistics was not used for 1nF/ 2kV capacitor, its ceramic composition is very similar to the 0.47 nF/ 3kV capacitor, and a BD strength of the order of 102 kV/cm was obtained in this case. Considering the thickness (0.68 mm and 1.18 mm) and the DC working voltage (2 kV and 3 kV), specified by manufacturer, gives a minimum DC BD voltage of about 30 kV/cm and 25 kV/cm, respectively, for 1.0 nF and 0.47 nF capacitors. This means that on pulsed conditions the dielectric can operate under BD strength three times superior than on DC. In addition, note in the polarization loops of Fig. 2 that the intensity of the AC electric fields used of 5.0 kV/cm and 22.0 kV/cm were respectively far less than the DC BD strength of the PZT and BT dielectrics tested.

2.3. Nonlinearity

The simplest way for checking the dielectric nonlinearity is by means of a C×V measurement made on static condition, where a C-meter reads strictly the differential capacitance of the dielectric under test, charged by a HV DC power supply. Measuring C×V curve on pulsed condition is also possible as demonstrated by Kuek et al. [15] but the discrepancies compared the last method employed are not so huge, in special when the capacitance saturates at higher voltages, which is the region of interest for calculating the RF oscillation frequency and output pulse rise time. Figs. 3 (a) and (b) illustrate the nonlinearity effect by showing the dependence of the capacitance and the corresponding permittivity versus applied voltage for PZT type 4 and BT-based capacitor of 1.0 nF/ 2 kV. As result, we obtain that BT-based dielectric are more nonlinear than PZT as the capacitance decreased 50 %

for the former and only 17 % for the latter when both submitted to maximum dielectric strengths of the same order (30 kV/cm and 27 kV/cm, respectively, for PZT and BT thicknesses of 2 mm and 0.68 mm).

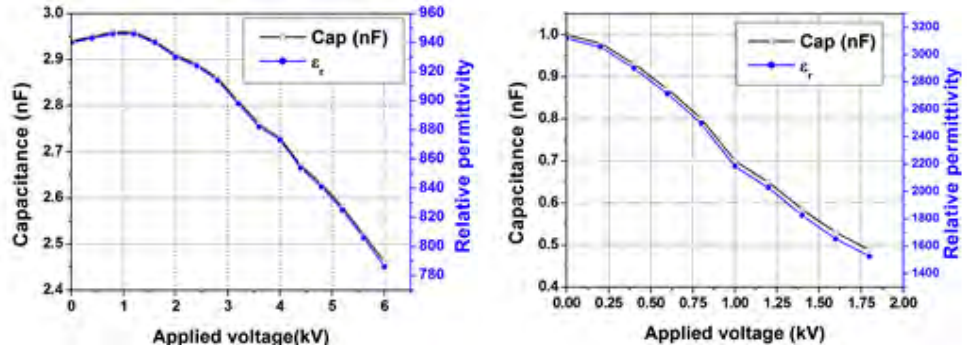

(a) (b)

Fig. 3. C×V measurement obtained for circular PZT type 4 (a) (left) and 1nF capacitor (right) (b).

Other way of checking dielectric nonlinearity is to produce a pulse discharge into a load from a NLTL employed as a pulse-forming network (PFN). In practice as a switch, we used a 2-electrode spark gap (SG) to discharge the line and a load matched to the unbiased line impedance. The SG initiated the discharge as the line charged voltage reached its breakdown at 1.6 kV, producing a pulse with peak amplitude of about 800 V at the load as expected. Figs. 4(a) and (b) shows the NLTLs built in oil and in air using circular PZT and 1 nF/2 kV ceramic capacitors, respectively. The lines were built with ten sections using air-core inductors of 1.0 μH. Figs. 5(a) and (b) show respectively the discharge pulse across the load. Because of the weak nonlinearity of PZT at 800 V, a rectangular pulse is formed as shown in Fig. 5 (a). However, for the ceramic capacitor line, the stronger nonlinearity of the BT distorts the output pulse, which has a longer fall time as shown in Fig. 5 (b). As pointed out by Smith and Bendixsen [16] the during pulse formation the top of the reflected voltage pulse travels faster along the line than its bottom distorting the voltage step into a ramp, which causes a long tail on the output pulse. In special for PZT, Spice simulation of a line with respective linear capacitors illustrates its weak nonlinearity as the experimental and Spice results are in good agreement (see black and red lines respectively in Fig. 5(a) again). However, as demonstrated by the experimental result by the red line in Fig. 5(a), linear capacitors used in Spice simulation (in blue) do not produce the correct result.

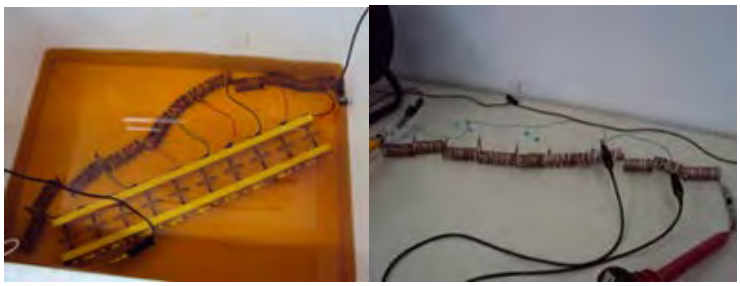

(a) (b)

Fig. 4. NLTLs built in oil with PZT (left) (a) and in air with ceramic capacitors (b).

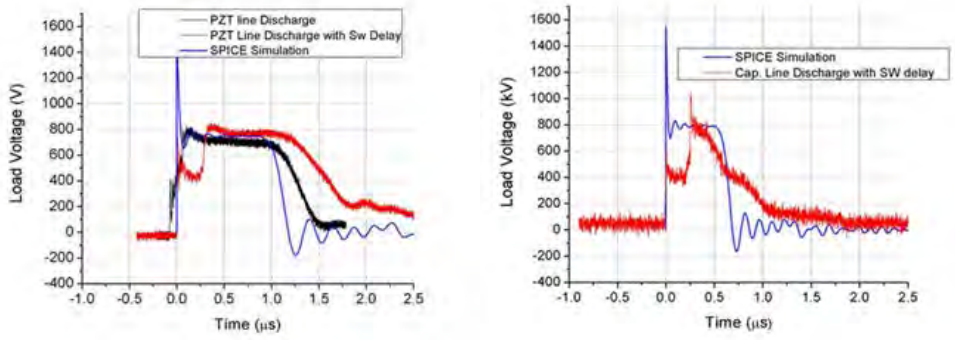

(a) (b)

Fig. 5. PZT (left) (a) and BT (right) (b) NLTL discharges in a matched load compared to the Spice simulations.

2.4. Frequency Response

A special attention to the frequency response of the ceramic dielectrics is needed. Using an HP RLC 4285A meter with bandwidth of 30 MHz the permittivity variation versus frequency is measured for the PZT (C#4 in blue line) and BT-based capacitors in a low frequency range as shown in Fig. 6.

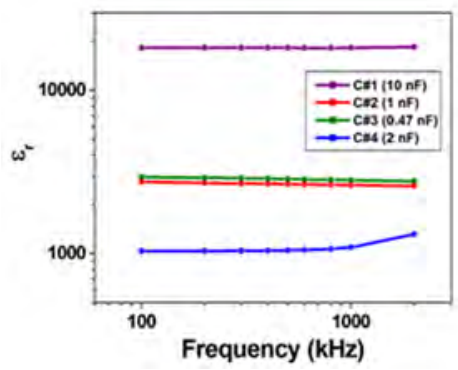

Fig. 6. Performance of permittivity versus frequency for PZT (in blue line) and BT-based capacitors [17].

This is an important parameter to be measured as permittivity must not drop with frequency if an input high frequency is injected into the line for producing a shockwave, otherwise the nonlinear effect cannot be explored. Nevertheless, resonant frequency caused by parasitic inductances due to component geometry or terminals limits the output frequency in NLTLs. As shown in Fig. 6, as expected the permittivity for all capacitors is approximately constant with frequency in the range measured. However, as seen in Fig. 6, ε_r tends to increase around 2 MHz for PZT because of their terminals used to couple to the input HP meter. Therefore, component resonant frequency is an important factor that affects NLTL performance at high frequency as dielectric loss tangent increases considerably at this point. At the resonant frequency, the capacitive reactance is compensated by the inductive reactance and the capacitor becomes an inductor above this frequency. This condition is illustrated in Fig. 7 as permittivity goes to negative values for PZT and BT-based capacitor (470 pF) at the resonant frequency around 200 MHz, where the permittivity measurements in high frequency sub-GHz range was made by measuring the complex reflection parameter $S_{11,}$ with the Agilent E8364B vector network analyzer (VNA) and terminal leads of the dielectrics removed.

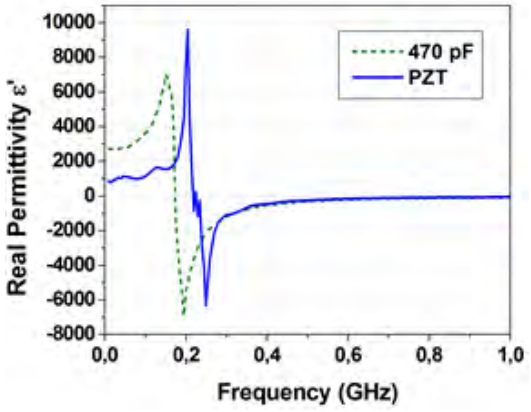

Fig. 7. Permittivity variation as function of frequency measured for PZT and 470 pF BT-based capacitors [7].

One can observe that dielectric losses are significantly lower far from the capacitor resonant frequency as shown in Fig. 8. At the resonant frequency, the loss tangent curves exhibit a peak as the capacitor behaves as a resistor since the net reactance is zero due to the associated parasitic inductance. For comparison, note that linear ceramic capacitors (100 pF and SMD) have significant lower losses than nonlinear capacitors (470 pF and PZT), especially at lower frequencies below 0.3 GHz. Also, observe that SMD does not present a loss peak because in the frequency range measured because of its extremely lower capacitance of 1.0 pF. Therefore, NLTL operation frequency of

PZT and BT can be limited up to the order of 200 MHz due to the loss peak at the resonant frequency caused by the inherent parasitic inductance. Estimated stray inductances for these dielectrics are in the range between 2.0 – 4.0 nH, approximately.

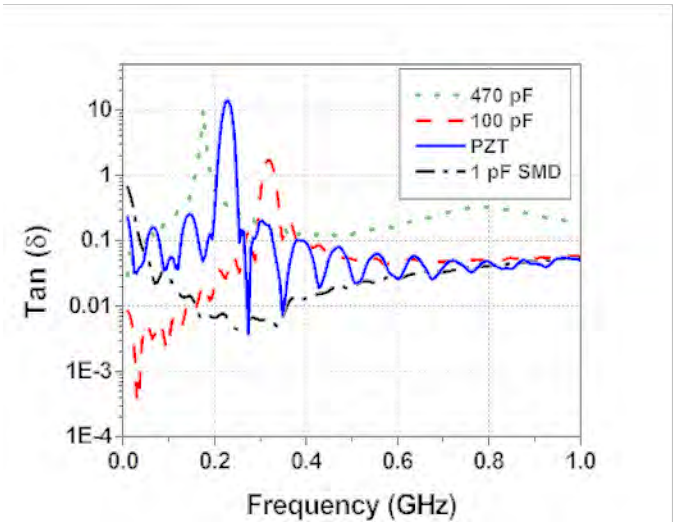

Fig. 8. Loss tangent calculated from S11 parameter versus frequency for all capacitors [7].

3. NLTL Principles of Operation for RF Generation

When an input pulse is injected into a dispersive LC line it propagates down the line length with a velocity given by $c = 1/(LC)^{1/2}$. If the line is nonlinear with variable capacitance C(V), the phase velocity is calculated by [18]:

$$V_p = 1/\sqrt{LC(V)}, \quad (1)$$

where C(V) is the variable capacitance per section as a function of the voltage applied, and L is the respective linear section inductance. The portion of the pulse with higher amplitudes will travel faster than its part with lower initial amplitude. In this way, the pulse peak catches up with the rising edge, forming an output shock wave front with a very fast rise time as shown in Fig. 9.

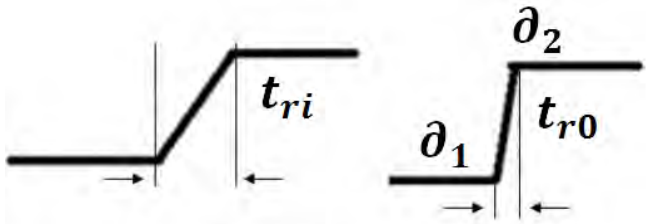

$$t_{ri} + \partial_2 - \partial_1 = t_{r0}$$

$$t_{ri} - t_{r0} = \partial_1 - \partial_2 = \Delta T$$

Fig. 9. Pulse rise time reduction in a NLTL.

A rough estimative for the pulse rise time reduction caused by the LC ladder sections is made by calculating the time delay difference between the lower amplitude portion and the peak of the propagation pulse as [18]:

$$\Delta T = t_{ri} - t_{ro} = \partial_1 - \partial_2 = n\left(\sqrt{LC_0} - \sqrt{LC(V_{max})}\right) = n(\sqrt{LC_0}(1 - \sqrt{k}), \quad (2)$$

where:

- t_{ri} is the input rise time,

- t_{ro} is the output rise time,

- n is the number of sections of the line,

-k is nonlinearity factor = $C(V_{max})/C_0$,

- C_0 is the unbiased capacitance,

- $C(V_{max})$ is the decreased capacitance at the maximum voltage applied,

- ∂_2 and ∂_1 are respectively the propagation delay times of the peak and lower amplitude portion of the input pulse, where $\partial_1 > \partial_2$.

A more accurate estimation is difficult because of the line nonlinearity. Then, the final rise time of the output compressed pulse (shock wave front) is calculated such as $t_{ro} = t_{ri} - \Delta T$, where $t_{ri} > \Delta T$. On the other hand, if t_{ri} starts to decrease so that $t_{ri} \approx \Delta T$, t_{ro} cannot decrease to zero as the steepness of the output shock wave would become infinite. Therefore, the pulse-rise time reduction is limited ultimately by the cutoff frequency of the biased LC ladder (known as Bragg frequency) as the line is dispersive, which is:

$$f_{CO} = 1 / \pi \sqrt{LC(V_{max})} \quad (3)$$

As the propagating pulse cannot be submitted to further sharpening for a high number of sections because the energy cannot propagate above f_{co}, the spectrum of frequencies from the shock wave is separated, producing at the output a series of narrow pulses (solitary waves) with frequency close to the half of the biased line Bragg frequency, that is $f=f_{co}/2$. As it will be shown in section 3.2, the biased line Bragg frequency varies along the line section because of the voltage reflections, depending on the load value. Other important line parameter is its characteristic impedance given as follows [18]:

$$Z_0 = \sqrt{L/C(V)} \tag{4}$$

According to (4) the impedance of the line generally increases with the voltage applied because of the capacitance decrease when ceramic capacitors or varactor diodes are used.

3.1. The Experimental Set-up and Spice Simulation

The NLTL was made on a phenolite PCB using 30 sections with linear inductors of L = 2.7 μH and the BB809 varactor diode as nonlinear capacitors [9], [19]. Fig. 10 shows the experimental set-up with the PCB NLTL and the TTI pulse generator (model TGP 110), on the right side, responsible for producing the rectangular input pump pulse and, the digital Tektronix oscilloscope, on the left side, used to display and store the input and output signals. BNC connectors and 50 Ω coaxial cables were also used to make the connections between the PCB and oscilloscope/pulse generator devices. The BB809 C×V curve obtained from manufacturer datasheet [20] is shown in Fig. 11. This curve can be modeled by a function given by [21]:

$$C(V) = C_{j0}/\left(1 + V/V_j\right)^m, \tag{5}$$

where V_j is the diode junction potential, m is the nonlinearity factor and C_{j0} is the unbiased diode junction capacitance.

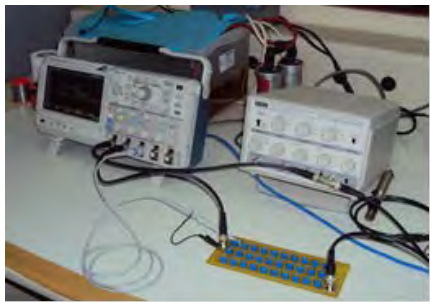

Fig. 10. Experimental set up for the NLTL tests.

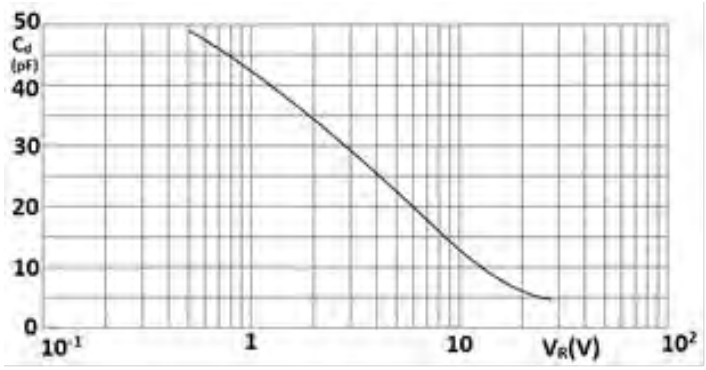

Fig. 11. Diode capacitance as function reverse applied voltage [21].

From the Fig. 11, one obtains that C_{j0} is of the order of 60 pF and C(Vmax) of about 15 pF, which gives 75 % variation for the capacitance decrease at 9 V. Other important parameters obtained from the datasheet are V_j= 0.7 V and m = 0.5. For the simulation model, it was used the NLTL diagram circuit shown in Fig. 12, including ohmic losses of L and C (respectively, R_L = 0.56 Ω and R_C = 6.8 Ω) and the BB809 varactor diode with parameters discussed previously in last paragraph. The simulation was done by using 30 sections in Spice circuit model to compare with the corresponding experimental results.

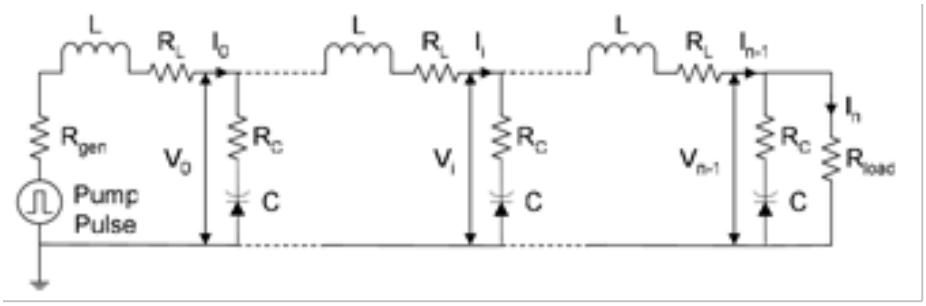

Fig. 12. NLTL schematic circuit used for NLTL simulation using BB809 varactor diodes.

3.2. RESULTS

A 50 Ω impedance pulse generator fed the line with a 9 V amplitude pump pulse of 310 ns duration and 15 ns pulse rise time. For maximum voltage amplitude of the pump pulse, the diode varactor gives C(Vmax) of about 15 pF. Using eq. (2) obtains Δt = 190 ns, which certifies production of oscillations at the line output since t_{ri} << Δt as discussed in section II. The experimental result confirmed that as shown in Fig. 13 (a) by the voltage oscillations on section 29 for a load of 1.0 kΩ and a delay time measured of the order of 200 ns. In this case, the value of load resistance is not matched to the circuit because greater the mismatch, greater the amplitudes of the oscillations at the output. In fact, the NLTL is never fully matched to the load as the line characteristic impedance (see eq. (4)) varies between the unbiased value of 212 Ω and biased one of 734 Ω with saturated capacitance of 5 pF as shown in Fig.11. The frequency of the oscillations obtained of about 40 MHz is close to the half of the biased line cutoff frequency of 43 MHz as expected. The NLTL Spice simulation obtained (shown in Fig. 13(b)) for voltage on section 29 is also in good agreement with the experimental result of Fig. 13(a), which demonstrates the validity of varactor diode model used in the Spice simulator [9], [19].

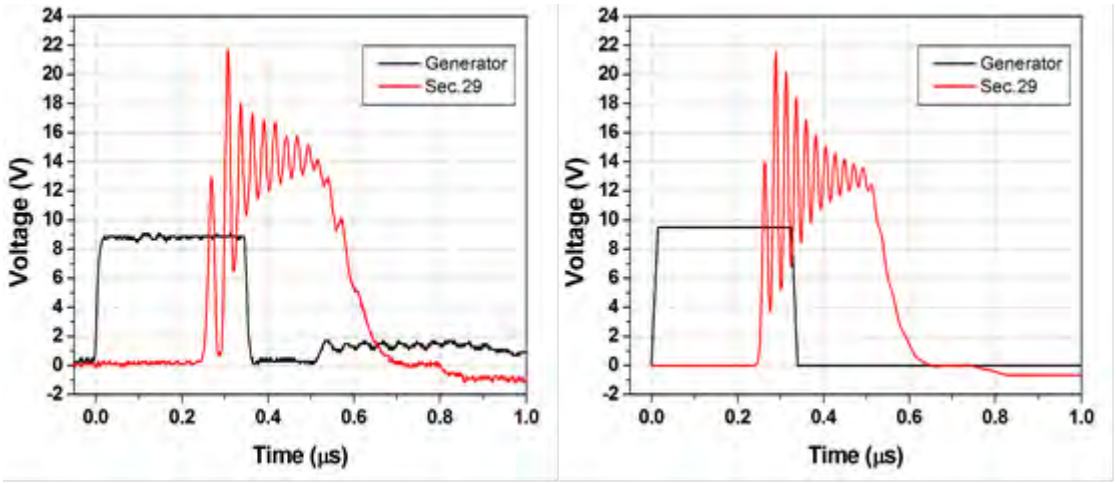

(a) (b)

Fig. 13. NLTL experimental (left) (a) and simulation (right) (b)results for pulse voltages on section 29.

Fig. 14(a) illustrates the pulse propagation along the line showing the pulse voltages on different sections of the NLTL (sections 5, 10, 20 and 29). The increase in the pulse amplitude on section 29 is due to the reflected pulse caused by the load mismatch (1 kΩ) with positive reflection coefficient. With higher resistive load, the

positive voltage reflection along the line does no cause significant variation on the oscillation frequency as the capacitance is near saturation for the input pulse amplitude of about 10 V. Therefore, the frequency of oscillations pratically does not vary with a higher load along the line as we can note in the transient response in Fig. 14(a). Fig. 14(b) shows the corresponding simulation results obtained with a good accuracy compared to the experimental case given in Fig. 14(a).

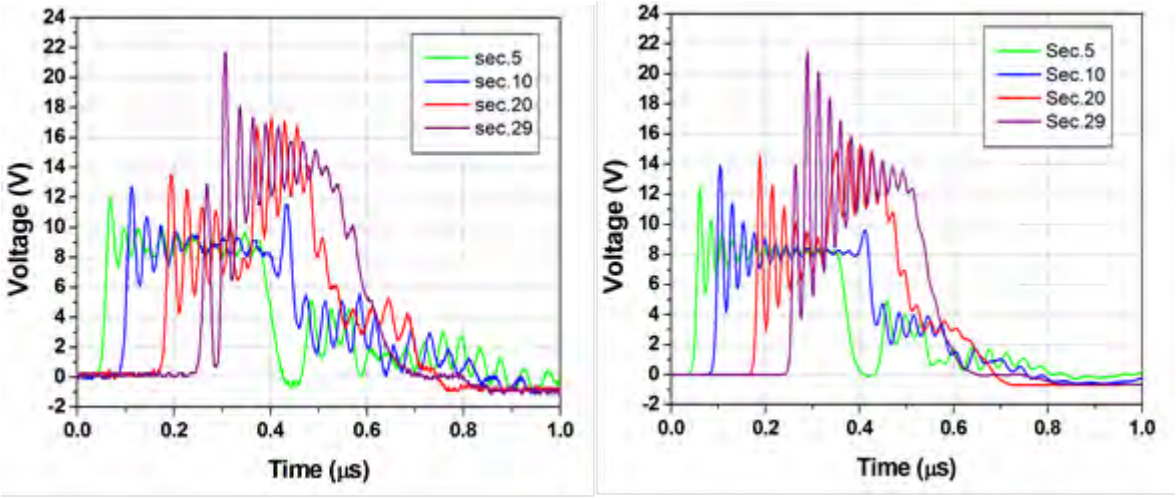

(a) (b)

Fig. 14. Experimental voltage pulse (a) (left) and Spice simulation (b) (right) obtained for the NLTL on different sections.

With the load, the Fig. 15(a) shows the effect of its variation on the voltage modulation depth (VMD) and the output oscillation frequency generated on the last section. It is clearly that for a higher resistive load (1 kΩ) above the unbiased line impaedance (210 Ω), the oscillation frequency increases and the VMD is slightly better for higher impedances. Also for lower loads, the DC level on the output pulse is reduced because of the negative voltage reflection at the load, which decreases the biased line Bragg frequency and in turn the oscilltation frequency as capacitance is increased. This is confirmed by the corresponding Spice simulations of the FFT spectra for all loads as displayed in Fig. 15(b), where one can notice that the oscillation frequency increases with higher loads shown by the lobes on the spectra. When load is reduced the ouput oscillation frequency tends to 30 MHz while in the opposite (load increase) the oscillation frequency tends to 43 MHz [9], [19].

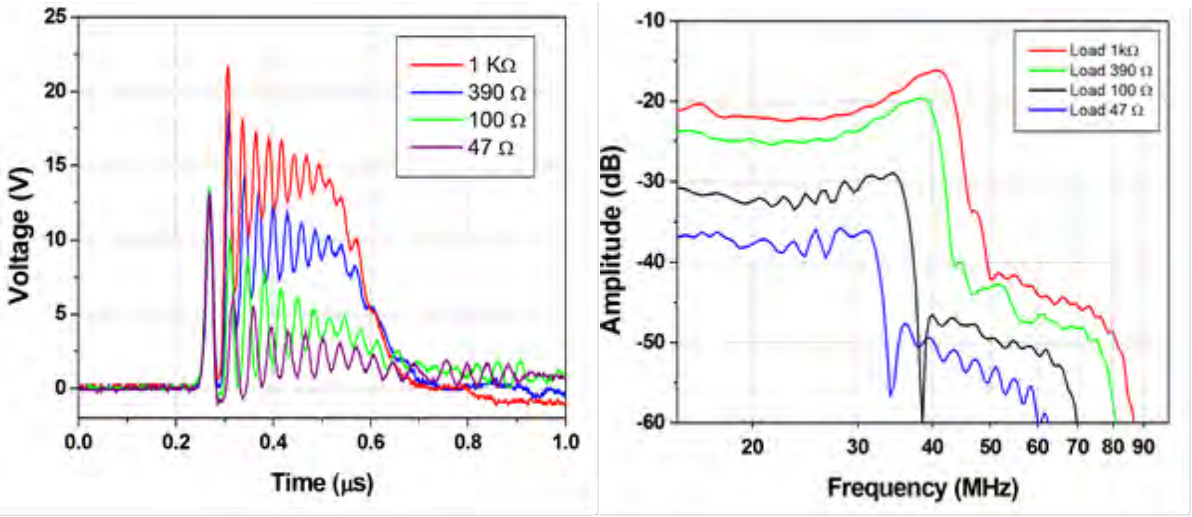

(a) (b)

Fig. 15. Variation effect of load resistance on secton 29 (a) (right) and corresponding FFT spectra simulated (b) (left).

As reported previously, although the output frequency does not vary much along the line with higher load as diode capacitance is near saturation, on the contrary oscillation frequency decreases along the line towards the output when load is much less than the unbiased line characteristic impedance. Fig. 16(a) gives the transient response of the output pulse of the NLTL on the 100 Ω load and on section 10. Corresponding FFTs in Fig. 16(b) show that on section 10 the oscillation frequency is of about 40 MHz while on load the frequency is around 28 MHz. The explanation for this is with sub-unmatched loads (<< 212 Ω), the DC level along the line is reduced, especially on the load, which increases the capacitance far from the saturation, reducing the oscillation frequency significantly towards the load. In comparison to higher loads, see in Fig. 14 (a) that DC level of the pulses increases on sections near the load because of the mismatch reflections caused by the load positive reflection coefficient [9], [19].

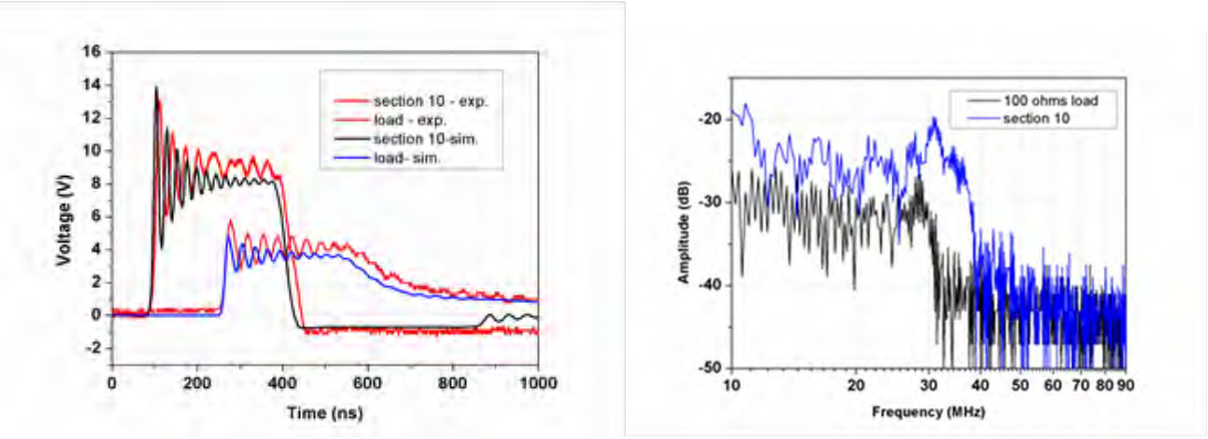

(a) (b)

Fig. 16. Voltage pulses on section 10 and on the load (a) (lfet) with corresponding FFT spectra (b) (right).

The experimental and simulation results of the output pulse for different number of sections employed in the PCB NLTL are shown in the Figs. 17(a) and (b), respectively, at a load of 1.0 kΩ using the same parameters of the pump input pulse of previous tests. As shown the simulations are in a good agreement with the experimental results and the oscillation frequency on load remains practically the same around 40 MHz, not depending on the number of sections. For the experimental results with 30 sections, the oscillations of the output signal are more attenuated than that of the corresponding simulation due to the increase of the ohmic losses in longer lines in practice. Moreover, as n becomes larger the number and amplitudes of oscillations as well as the line delay time increase as shown in Figs. 17(a) and (b). However, for the case tested, optimum n lays between 20 and 30 as the number of oscillations are limited by the input pulse duration set at 300 ns [9], [19].

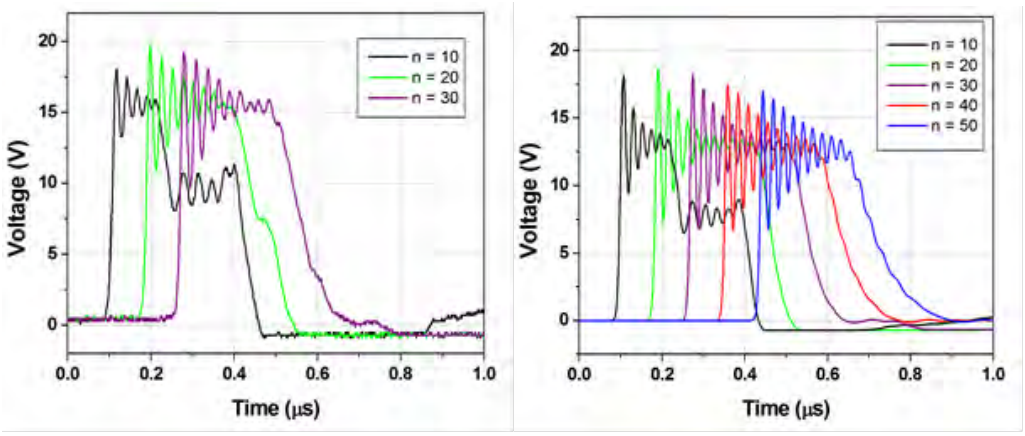

(a) (b)

Fig. 17. Effect of the NLTL n increase on the output pulse (a)) (lfet) and corresponding Spice simulation up to 50 (b) (right).

The maximum voltage of generator, which reached only 12 V, limited the pulse amplitude applied of 10 V to the line input. The influence of the pump input pulse amplitude on the output oscillations was investigated for three different values (1 V, 5 V and 10 V) as shown by the NLTL output pulses in Fig. 18(a). We can see that low voltage amplitudes do not produce noticeable oscillations, as nonlinearity is too low to cause significant capacitance decrease. This experimental result also demonstrates that frequency tuning is achieved by controlling the pump pulse amplitude, as frequency of oscillations varies approximately between 25 and 40 MHz for a corresponding variation of amplitude in the range of 5-10 V. Spice simulations can produce similar results by varying the pump pulse amplitude in 5 V steps above 5 V (see Fig. 18(b)). However, as seen in simulations, above 20 V, distortion and attenuation on the output pulse oscillations start to degrade the system efficiency as amplitude approaches the diode reverse breakdown voltage of 30 V, with greater attenuation at 25 V amplitude. Anyway, using higher pump pulse amplitudes up to certain value below the diode breakdown voltage is an excellent way to increase oscillation frequency. In Fig. 18(b), 15 V amplitude is the best case simulated for the generation of RF oscillations with lower attenuation and better VMD at 50 MHz approximately [9], [19].

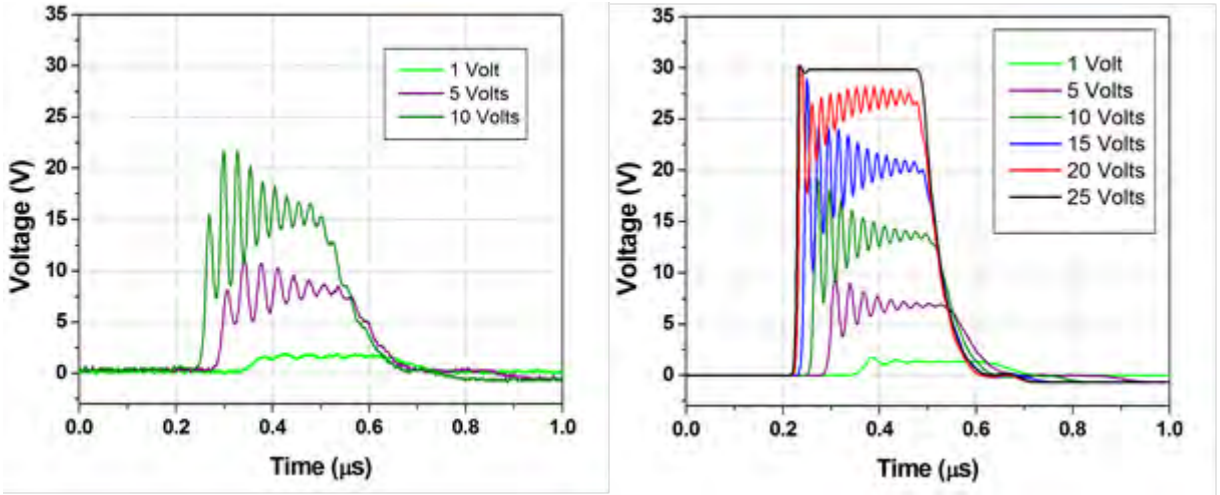

Fig. 18. Effect of the pump pulse amplitude on the output oscillations (a) (left) and correposding Spice simulation up 25 V (b) (right).

4. The HV Capacitive Nonlinear Line (NLCL)

In this work, it is described the implementation of a high voltage nonlinear capacitive line (NLCL) using BT and PZT ceramic capacitors. Corresponding NLCL Spice simulation are also provided for comparison with experimental results.This section discusses the minimum input pulse rise time to achieve RF generation with pulse compression at the output.

4.1. The Schematic circuit of the NLCL

The NLCL schematic circuit to feed the NLCL is shown in Fig. 19. A pump input pulse generator is required to inject a rectangular pulse into the line. The pump pulse generator consists of a storage capacitor (C1//C2) and a high voltage (HV) switch (an IGBT transistor with holding-off capability of 1.2 kV). As shown in Fig. 19, a DC high voltage source acquired from Gamma Company charges the storage capacitors up to the nominal voltage and a low voltage pulse generator triggers the HV switch to discharge the storage capacitor for producing the pump input pulse. This input pulse travels along the line and emerges with faster rise time delayed at the output on a resistive load of 70-80 ohms. An input series resistor of 33 ohms placed bewteen the switch and the line is used to limit the IGBT current. The high voltage diodes D5 to D10 are used to protect the HV switch against negative back swing voltage, while D4 diode for reverse current. Because of the HV circuit configuration, a pulse transformer is used to isolate the pulse trigger pulse generator from the IGBT gate. In this work, three NLCLs were constructed using ceramic BT and PZT ceramic capacitors with linear inductance of 3.3 μH. The same configuration was used for the corresponding Spice simulations. Fig. 20 shows a picture of a 30-section NLCL constructed with BT ceramic capacitors.

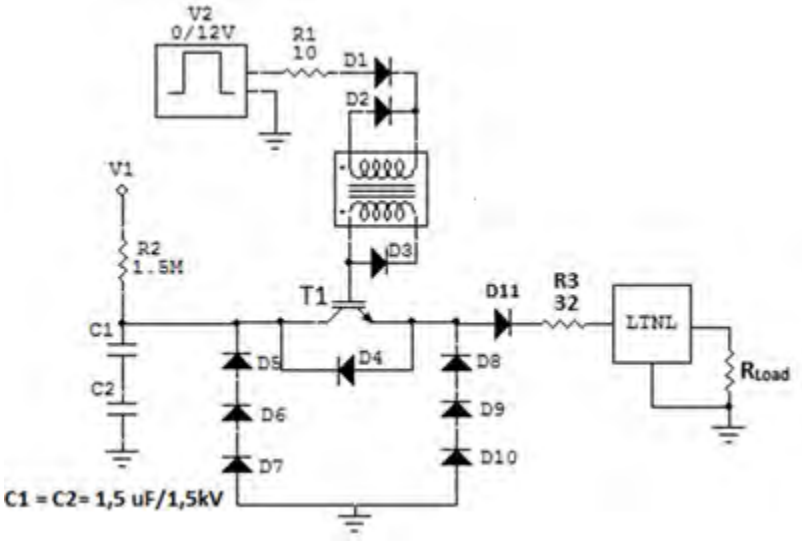

Fig. 19. Electrical circuit with IGBT switch used to test the NLCL.

Fig. 20. Picture of the 30-section NLCL PCB built with BT ceramic capacitors.

4.2 BT NLCL Experimental Results

For this line, two commercial-off-the-shelf ceramic capacitors (COTS) with strong nonlinearity were selected according to Table I. The commercial capacitors have dielectric mixture in which the main compound is the barium titanate ($BaTiO_3$) [22]. Based on US EIA standards, capacitor C#1 is of 1 nF with Y5U dielectric (capacitance tolerance of +22 % to -56 %) and C#2 is of 10 nF with Y5V dielectric (+22 % to -82 %) over a temperature range between -30 °C and +85 °C.

Table I. Electrical Characteristics of the BT ceramic capacitors tested.

Sample	Capacitance (nF)	Dielectric type	Nom. Voltage (kV)
C#1	1.0	(Y5U)	2.0
C#2	10.0	(Y5V)	2.0

The experimental output signal in the line using C#1 confirms that the pulse rise at the output on a 70-ohm load is slightly compressed as shown by the brown line in Fig. 21 since $t_{ri} > \Delta T$, where t_{ri} measured is of about 2.5 μs (see green line) and pulse rise rime reduction calculated of 660 ns. Due to the longer rise-time of the input pulse driver caused by the slower IGBT switching time, ΔT is not enough to approach t_{ri} for causing RF oscillations as explained in section 3. We can see from eq. (2) (see section 3) that the value of ΔT depends on the unbiased capacitance, nonlinearity factor, inductance and number of sections n. Since the same input pulse driver was used for the test as well as the same number of sections and inductance in the NLCL, the use of the line capacitor C#2 of higher capacitance and stronger nonlinearity produces RF oscillations on an 82-ohm load as illustrated in Fig. 22 by the red line. Observe that the rise time of input pulse is still in the microsecond range (blue line) but in contrast to the previous case, the pulse rise time reduction factor calculated now is higher ($\Delta T = 3.27$ μs > $t_i = 2.0$ μs), which explains the RF formation according to the theory described in the introductory part of section 3.

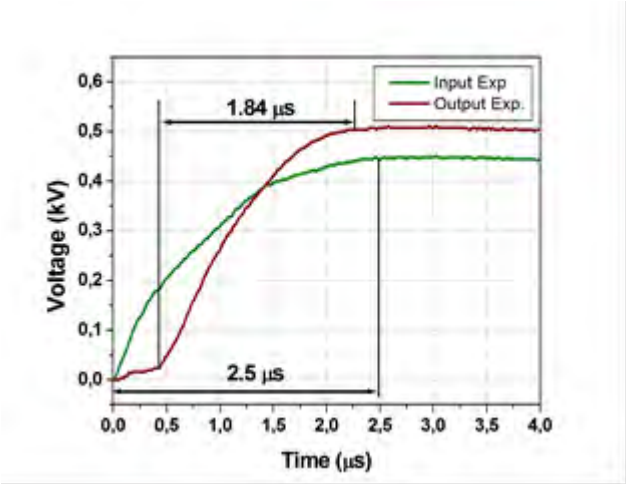

Fig. 21. Experimental waveforms showing pulse sharpening obtained at the output of line using C#1.

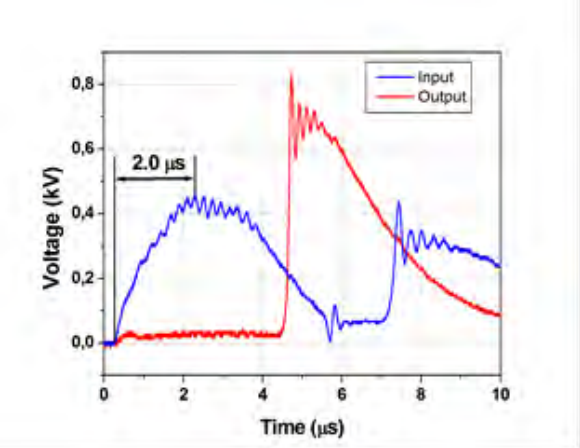

Fig. 22. RF soliton generation at line output using capacitor C#2.

Other interesting results are shown in Fig. 23 by the RF formation along the C#2 line, where one can observe that the modulation depth of the oscillations are higher on the line middle sections since the RF intensity at the load is normallly lower in NLCLs. Also Fig. 24 gives the corresponding dependence of the RF oscillations on the pulse amplitude since line nonlineariry is weaker with lower voltages, where the input pulse amplitude is controlled through the capacitor charging voltage.

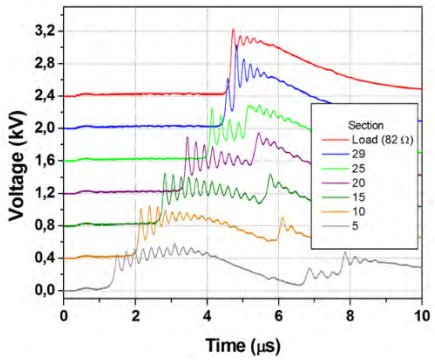

Fig. 23. Illustration of the RF formation along the C#2 NLCL.

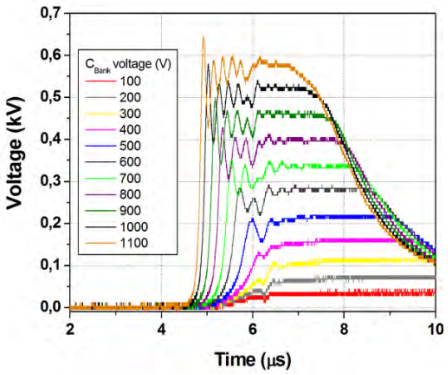

Fig. 24. Dependence of RF formation on the input pulse amplitude.

As shown by previous results, the nonlinearity factor of ceramic capacitors is an inportant factor to be measured for obtaining RF oscillations. By using the experimental curves C×V given in Figs. 25 and 26, one can measure the nolinearity factor of capacitors C#1 and C#2 as k = 0.5 and 0.1, respectively. In both figures, the sacttered points represent the capacitance measured under DC condition. The good fiiting obtained betwwen the experimental points and the solid line was obtained modeling the capacitance as an hyperbolic function given by [21]:

$$C(V) = (C_0 - C_1) \cdot \left[1 - \tanh^2 \left(\frac{V}{V_1} \right) \right] + C_1, \tag{5}$$

where C(V) is the capacitance at the full pulse amplitude, C_0 is the unbiased capacitance, and C_1 and V_1 are the fitting parameters. .For the theoretical fitting curve of capacitor C#1 in Fig. 25, we used the values C_0 = 1.0 nF, V_1 = 1.2 kV e C1 = 0.4 nF to obtain a good agreement between experiment and modeling. For C#2 in Fig. 26, the fitting parameters were C_0 = 7.5 nF, V_1 = 0.4 kV and C_1 = 0.7 nF.

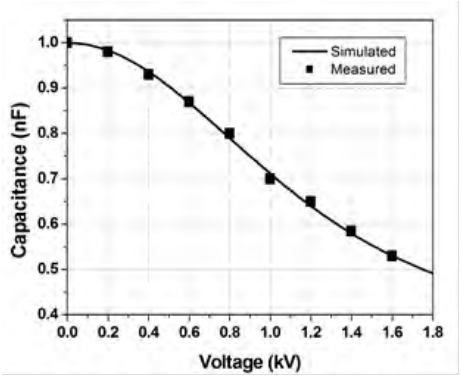

Fig. 25. The C×V characteristic curve of Capacitor C#1.

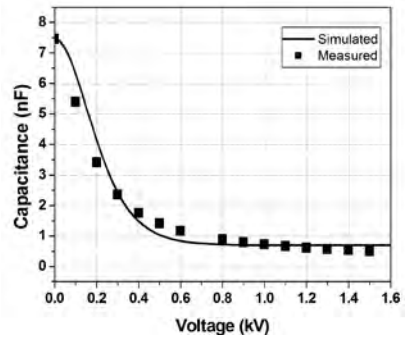

Fig. 26. The C×V characteristic curve of Capacitor C#2.

Finally, Fig. 27 shows the FFT spectrum measured for the experimental waveform of the output pulse (see Fig. 22) confirming that RF frequency generated is of the order of half of the Bragg frequency (about 3.3 MHz). This value is according to the calculation provided by $f=f_{co}/2$ with n=30 (see eq. (3) again), considering the linear inductance of 3.3 μH and saturated capacitance of 0.7 nF for C#2 (see Fig. 26).

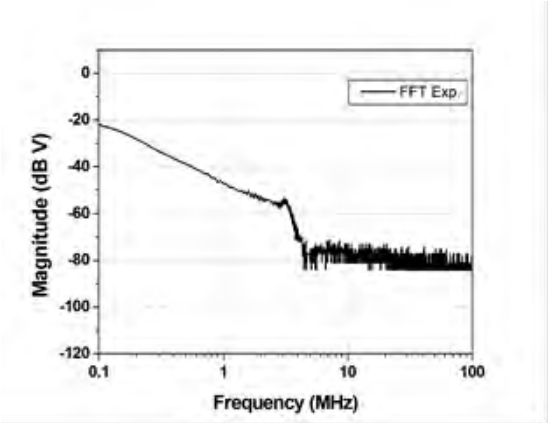

Fig. 27. FFT spectrum measured for the output pulse given by the red line in Fig. 22.

4.3 BT NLCL SPICE SIMULATIONS

Using the ladder model of C#1 as shown in Fig. 12 to simulate the NLCL in the LT-Spice circuit simulator, a sharpened pulse is obtained at the output of the line as shown in Fig. 28. The blue line represents the input pulse with rise time of the order of 2.8 μs and the red line represents the output pulse obtained on the load (82 Ω) with rise time of 2.2 μs. In order to obtain a good fitting, the line capacitor parameters obtained were measured under dynamic conditions from the C-V curve [23]. In particular, for these simulations the values used for C#1 given by the modeling eq. (5) were C_0 = 0.5 nF and C_1 = 0.1 nF with V_1 = 650V for an ideal switch with internal inductance of 50 μH. During the capacitor discharge, as noted by Siang [15], the unbiased capacitance, saturation voltage and capacitance measured on dynamic tests (C_0, V_1 and C_1, respectively) are much lower than measured under DC static condition in Fig. 25. Using these values of C_0 = 0.5 nF and C_1= 0.1 nF into eq. (2) one obtains a pulse rise-time reduction of the order 670 ns, very near the values obtained from the experiment (660 ns) and simulation (600 ns).

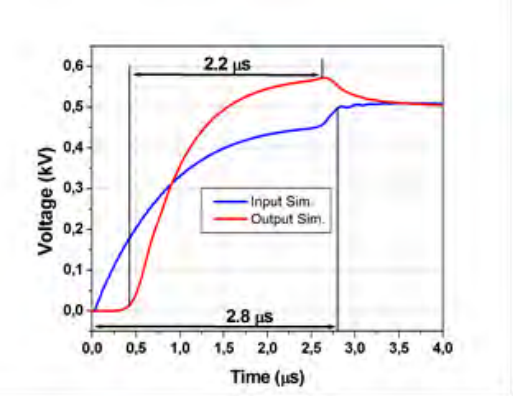

Fig. 28. Simulation result showing pulse sharpening at the NLCL output using C#1.

An important experimental observation was to consider the variation of the switch parameter on LT simulation. When the switch inductance was decreased from 30 µH to 1.0 µH, a faster input pulse rise time of the order of few ns (<< ΔT) was obtained according to Fig. 29. In this case, the output pulse rise-time is limited by the cutoff frequency of the lumped line, as the output front slope cannot become infinite or negative. As a result, the simulated output pulse emerges delayed at the load, and is broken into a train of solitons superimposed on its full amplitude as seen in Fig. 29. In this case, because of the weak nonlinearity of the capacitor used in the line, the amplitudes of oscillations are not high enough and they die away after only three cycles. This simulation result is very important for the NLCL design since it demonstrates the importance of obtaining fast switching (few ns or less) for soliton generation in nonlinear transmission lines with weak nonlinearity. The corresponding FFT spectrum of the output waveform is given in Fig. 30, showing a generated RF soliton frequency of about 4 MHz.

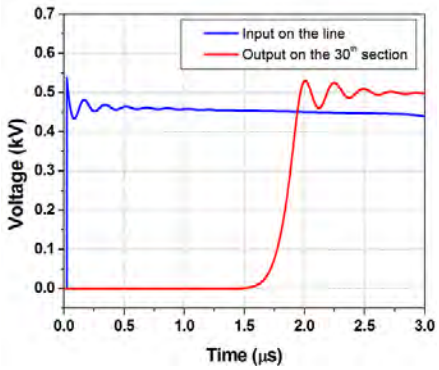

Fig. 29. Soliton generation in the NLCL using faster switching and C#1 as nonlinear capacitor.

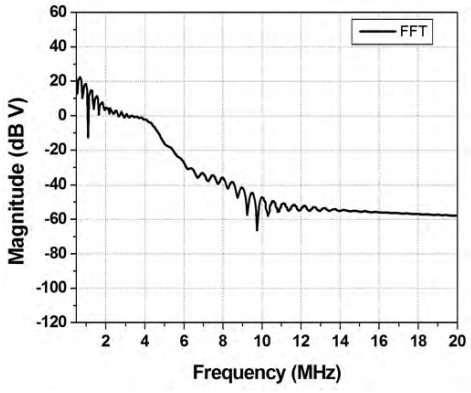

Fig. 30. Corresponding FFT spectrum simulated for the output voltage waveform using capacitor C#1 with faster input rise time.

Using C#2 as nonlinear element in the simulation of the NLTL, soliton generation is obtained at the output of the line according to simulation in Fig. 31 as the input pulse rise-time $t_{ri} \approx 2$ μs is shorter than the pulse rise time reduction factor $\Delta T = 3.27$ μs

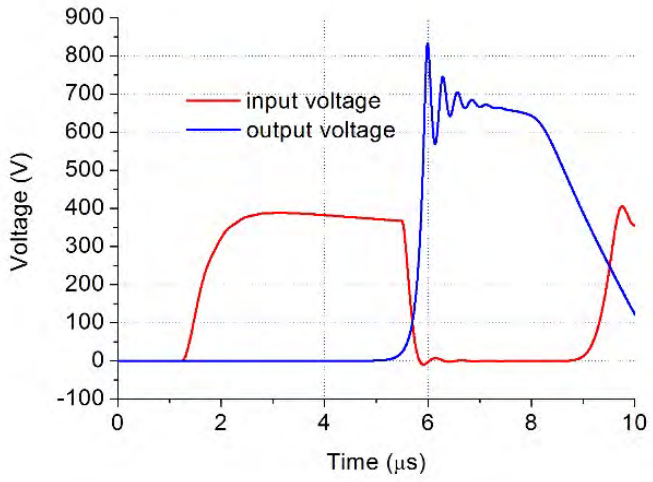

Fig. 31. Simulation results showing soliton generation at the NLCL output using C#2 and corresponding input voltage.

The corresponding FFT simulation of the output pulse voltage shown in Fig. 32 confirms the soliton generation frequency around 3.3 MHz, which is close agreement with the experimental value obtained from FFT in Fig. 27.

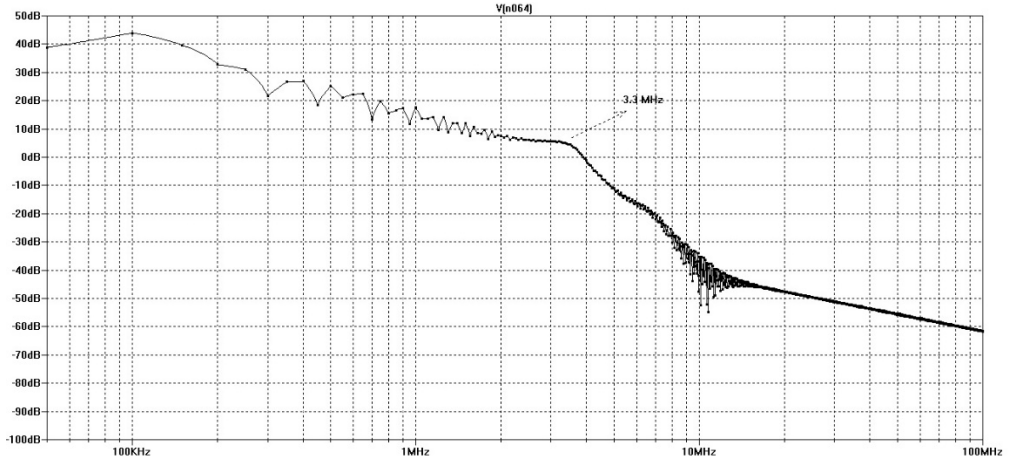

Fig. 32. Corresponding FFT spectrum simulated for the output pulse waveform using capacitor C#2.

4.4 PZT NLCL Experimental Results

In view of the previous results with BT ceramic capacitors with weak nonlinearity, circular type PZT-4 capacitors with larger dielectric thickness (2 mm) are not enough nonlinear for applications in NLTLs when operating far from their BD voltage (see Fig. 3(a) in section 2.3). However, near BD voltage they present nonlinearity (NL) factor $k \approx 0.5$ as illustrated in Fig. 33 by the decrease of the capacitance with voltage, where thinner PZT type-4 (0.5 mm thickness) with square shape (10×10 mm) were used for these tests [7]. Thus, the solution for using PZT in NLTLs is to operate the line with higher voltage, with dielectric strength slightly below the BD. To reduce dependence on using voltages above 5 kV the main idea is to use thinner PZT slabs (< 1 mm) in order to obtain higher dielectric strength close to their BD voltage.

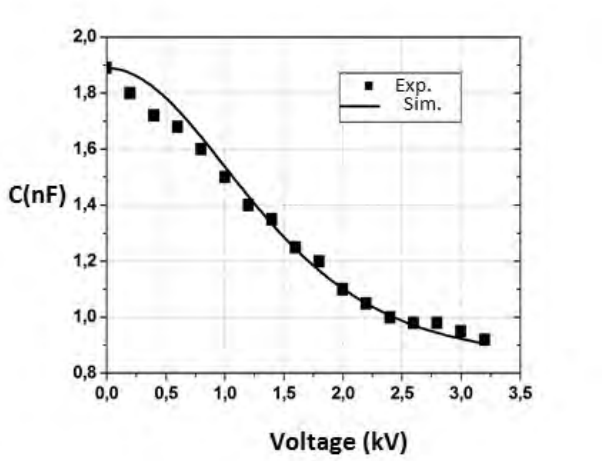

Fig. 33. C×V characteristic curve of the square shape PZT with thinner thickness.

However, when the NLCL was tested with 10 sections using the thinner squared shaped PZT and L=3.3 μH only pulse compression (see Fig. 34) without any RF oscillation was obtained on a 82 ohms load as expected because of the slower pump impulse driver employed. For the experimental result in Fig. 34, we can see that the input rise time is of the order of 3.2 μs while the output rise time of about 2.5 μs, leading to pulse rise time reduction of 700 ns approximately. It is surprising that this value is very close to that obtained with the 1.0 nF capacitor of weak nonlinearity in Fig. 21, which can be explained by the fact that, although the PZT line has only 10 sections, its unbiased capacitance is higher (see Fig. 33). For both cases, pulse rise reduction is of the order of the delay line and its calculation from eq. (2) cannot be promptly obtained from the C×V curve characteristic measured on DC condition. However, this calculation can be made using the C×V measurement on dynamic conditions in Spice simulations as shown in the previous section for the BT C#1 NLCL (see Fig. 28). This output pulse compression of the order of the line delay is not fully understood and further investigation on this phenomenon is needed. Anyway, the results obtained so far indicate that ceramic capacitors of weak nonlinearity (BT or PZT) can produce pulse compression. Besides that, probably they can even produce generate RF soliton oscillations if a faster pump input pulse driver is used as demonstrated in the previous section according to Fig. 29.

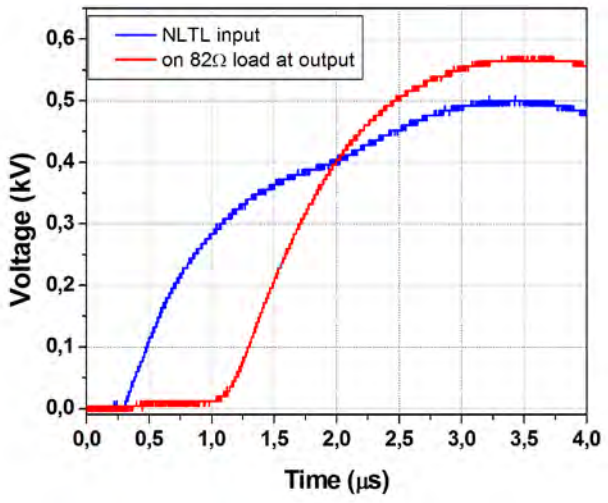

Fig. 34. Input and output experimental waveforms obtained from the PZT NLCL showing small pulse sharpening.

5. CONCLUSIONS

Pulse sharpening and soliton RF generation were achieved using ladder-type NLCLs. Using ceramic capacitors (BT and PZT) of weak nonlinearity (k=0.5), only pulse compression was observed for an input rise time in the microsecond range. The pulse rise reduction obtained was of order of 700 ns for the sharpened output pulse, in good agreement with simulation results. Herein, an important observation is that parameters of weak nonlinear capacitors such unbiased capacitance, voltage and capacitance at saturation seem to be much lower when submitted to the pulsed conditions as confirmed by the results, a phenomenon that must be investigated further. Nevertheless, using ceramic capacitors of stronger nonlinearity (k=0.1) soliton oscillations were generated at a frequency of 3.3 MHz approximately. Besides, through simulation using a low inductance switch for producing faster rise times, soliton generation was demonstrated to be possible even with the use of capacitors of weak nonlinearity in the NLCL. This is an important achievement once PZTs could be used for soliton generation, probably leading to better voltage modulation depth as they have lower dielectric losses than BT dielectrics. Other solution to improve the feasibility of the weak nonlinearity line could be use of a hybrid configuration with extra nonlinear elements at the same time such as saturated inductors. This research approach raises the need for characterization of magnetic ferrite beads [23] employed as nonlinear medium in hybrid NLTLs. Anyway, for lumped NLCLs beyond the nonlinearity factor other problem is the resonant frequency of the ceramic dielectrics that limits their application up to 200 MHz approximately, as shown in section 2.4. A solution for checking this limit for the NLCL operation could be use of a low voltage varactor diode line (shown in section 3) since the adverse effect of the stray inductances on line frequency performance is worse for tests with HV pulses. Finally, the more important aspect confirmed through simulations is that dielectrics with strong nonlinearity factor (k< 0.1) is an important issue for producing soliton RF combined with faster input pulse rise times in the range of few ns or less.

References

1) N. S. Kuek, A. C. Liew, E. Schamiloglu, and J. O. Rossi, “Circuit modeling of nonlinear lumped element transmission lines including hybrid lines,” IEEE Trans. Plasma Sci., vol. 40, n. 10, pp. 2523- 2534, Oct. 2012.

2) J. D. C. Darling and P. W. Smith, “High-power pulsed RF extraction from nonlinear lumped element transmission lines,” IEEE Trans. Plasma Sci., vol. 36, n. 5, pp. 2598-2603, Oct. 2008.

3) F.S. Yamasaki, L.P. Silva Neto, J.O. Rossi, J.J. Barroso “Soliton Generation Using Nonlinear Transmission Lines, IEEE Transactions on Plasma Science, v. 43, no. 11, pp. 3471- 3477, Nov. 2014.

4) J. O. Rossi, L. P. Silva Neto, and A. R. Silva Junior, “Study of HV dielectric ceramics for applications in compact pulsed power,” in Proc of the IEEE Int. Pulsed Power Conf. (PPC), Chicago, IL, 2011, pp

5) L. P. Silva Neto, J. O. Rossi, and A. R. Silva Junior, “Characterization of dielectric properties of commercial ceramic capacitors for pulsed power applications,” in Proc. of the Power Electonics. Conf. (COBEP), Natal, RN, 2011, pp. 347-351.

6) L. P. Silva Neto, J. O. Rossi, J. J. Barroso, A. R. Silva Junior, P. J. Castro, and P. A. G. Dias, “Characterization of ceramic dielectrics for sub-GHz applications in nonlinear transmission lines,” in Proc. of the SBMO/IEEE MTT-S Int. Microwave & Optolectronics Conf. (IMOC), Rio de Janeiro, RJ, 2013, pp. 1-5.

7) L.P. Silva Neto, J.O. Rossi, J.J. Barroso, A.R. Silva. “Characterization of Ceramic Dielectrics for Sub-GHz Applications in Nonlinear Transmission Lines”, IEEE Transactions on Plasma Science, v. 42, no. 10, p. 3274-3282, Oct. 2014.

8) J. D. Darling & P. W. Smith, “High power RF generation from non-linear delay lines,” in Proc. of the IEEE Int. PPC, Albuquerque, NM, June 2007, pp. 472-475.

9) J.O. Rossi, L.P. Silva Neto, F.S. Yamasaki, “Key Issues in Design of NLTLs,” Proc. of the 41st IEEE International Conference on Plasma Science/Beams, Washington, DC, USA, May 2014, pp. 1-6.

10) M.P. Brown and P.W. Smith, “High power, pulsed soliton generation at aadio & microwave frequencies”, in Proc. of IEEE Int. PPC, Baltimore, MD, June 1997, pp. 346-354.

11) H. Ikezi, J. S. DeGrassie, and J. Drake, “Soliton generation at 10 MW level in the very high frequency band,” Appl. Phys. Lett., vol.58, pp. 986-987, March 1991.

12) J.O. Rossi, L.P. Silva Neto, F.S. Yamasaki, and E. Schamiloglu, “Prospects of building capacitive nonlinear lines using ceramic PZT for high frequency operation”, ”, in Proc. of the IEEE Int. Pulsed Power Conf. (PPC), San Diego, CA, 2012, pp. 752-755.

13) Burfoot, J.C. and Taylor, G.W., “Polar Dielectrics and Their Applications”, Berkeley: University of California Press, 1979, p. 39.

14) L. P. Silva Neto, J. O. Rossi, and A. R. Silva Junior, “Characterization of dielectric properties of commercial ceramic capacitors for pulsed power applications”, in Proc. of the Power Electr. Conf. (COBEP), Natal, RN, 2011, pp. 347-351.

15) N.S. Kuek, A.C. Liew, E. Schamiloglu, and J.O. Rossi, “Pulsed RF oscillations on a linear capacitive line” IEEE Trans. Dielec. Eletr. Insul., vol. 24, no. 4, pp. 1129-1135, Aug. 2013.

16) L.S.C. Bendixsen, and P.W. Smith, “Very low impedance pulse forming lines built from ferroelectric tiles”, in Proc. of the IEEE Int. Pulsed Power Conf. (PPC), Monterey, CA, 2005, pp. 1333-1336.

17) L.P. Silva Neto and J.O. Rossi, “PZT dielectric ceramic characterization for application in nonlinear transmission lines,” Adv. Mat. Res., vol. 975, p.23-28, July 2014.

18) P. W. Smith, “Transient electronics – pulsed circuit technology”, John Wiley & Sons, West Sussex, England, 2002, p. 245-249.

19) L.P. Silva Neto, J.O. Rossi, J.J. Barroso, and F.S. Yamasaki, “RF pulse formation in NLTLs using varactor diode,” Proc. of the Symposium of Operational Applications in Areas of Defense (SIGE), DCTA, S.J. Campos, SP, Sept. 2014, pp. 43-48.

20) Philips, “BB809 VHF variable capacitance diode,” Philips semiconductor, pp. 1-4, May 1996.

21) F. S. Yamasaki, J. O. Rossi, J. J. Barroso, “RF generation using nonlinear transmission lines for aerospace applications,” In: SBMO/IEEE MTTS Int. Microwave and Optoelectronics Conf., R.J., 2013, pp. 1-5.

22) P. W. Smith, “Pulsed, high Power, RF generation from nonlinear dielectric ladder networks- performance limits”, in Proc. of the 18th International Pulsed Power Conference, 2011, pp. 167-172.

23) L.P. Silva Neto, J.O. Rossi, P.A.G. Dias, and J.J. Barroso, “Frequency Characterization of Ferrite Beads in the Microwave Range for Nonlinear Applications,” Materials Science Forum, v.802, pp.552 - 557, Dec. 2014

Main Publications Acknowledging AFOSR Support Result From This Grant

1) L.P. Silva Neto, J.O. Rossi, and A.R. Silva, “Applications of PZT dielectric ceramics in high-energy storage systems,” Materials Science Forum, v. 727-728, pp. 505-510, 2012.
2) J.O. Rossi, L.P. Silva Neto, F.S. Yamasaki, and E. Schamiloglu, “Prospects of building capacitive nonlinear lines using ceramic PZT for high-frequency operation. Proc. of the 2012 IEEE International Power Modulator and High Voltage Conference (IPMHVC), San Diego, May 2012, p.752 -755.
3) N.S. Kuek, A.C. Liew, E. Schamiloglu, and J.O. Rossi, “Oscillating pulse generator based on a nonlinear inductive line,” IEEE Trans. Pla. Sci., v. 41, p. 2619-2624, 2013.
4) N.S. Kuek, A.C. Liew, E. Schamiloglu, and J.O. Rossi, “Pulsed RF oscillations on a nonlinear capacitive transmission line,” IEEE Trans. Diel. Elec. Ins., v. 20, pp. 1129-1135, Aug. 2013.
5) F.S. Yamasaki, “RF generation for aerospace applications using nonlinear transmission lines,” M.Sc. thesis, INPE, São José dos Campos, SP, Brazil, Feb. 2013 (in Portuguese).
6) A.R. Silva, J.O. Rossi, M. Ueda, and L.P.S. Neto, “Adherence Enhancement of Metallic Film on PZT Type Ceramic Using Nitrogen Plasma Implantation,” Proc. of the 19th IEEE International Pulsed Power Conference, San Francisco, CA. June 2013, pp. 1-4.
7) J.O. Rossi, L.P.S. Neto, and R.H.M. Siqueira, “Study of the Ceramic Capacitor Dielectric for Pulsed Power,” Proc. of the IEEE 19th International Pulsed Power Conference, San Francisco, CA, June 2013, pp. 1-4.

8) N.S. Kuek, A.C. Liew, E. Schamiloglu,and J.O. Rossi, “Generating RF pulses using a nonlinear hybrid line,” Proc. of the IEEE 19th International Pulsed Power Conference, San Francisco, CA, June 2013. pp. 1-5.

9) J.O. Rossi, E. Schamiloglu, N.S. Kuek, and F.S. Yamasaki, “Design considerations in lossy dielectric nonlinear transmission lines,” Proc. of the IEEE 19th International Pulsed Power Conference, San Francisco, CA, June 2013, pp. 1-5.

10) J.O. Rossi, L.P. Silva Neto, F.S. Yamasaki, and J.J. Barroso, “State of the art of nonlinear transmission lines for applications in high power microwaves,” Proc. of the SBMO/IEEE MTT-S International Microwave and Optoelectronics Conference, Rio de Janeiro, Brazil, Aug. 2013, pp. 1-5.

11) L.P. Silva Neto, J.O. Rossi, J.J. Barroso, A.R. Silva, P.J. Castro, and P.A.G. Dias, “Characterization of ceramic dielectrics for sub-GHz applications in nonlinear transmission lines,” Proc. of the SBMO/IEEE MTT-S International Microwave and Optoelectronics Conference, Rio de Janeiro, Brazil, Aug. 2013, pp. 1-5.

12) F.S. Yamasaki, J.O. Rossi, and J.J. Barroso, “Study of nonlinear lumped element transmission Lines for RF generation,” Proc. of the Fourth Workshop on Engineering and Space Technology (2013 WETE), S.J Campos, SP, Brazil, Aug. 2013.

13) L.P. Silva Neto, P.A.G. Dias, J.O. Rossi, and J.J. Barroso, “Characterization of Radial and Ceramic Capacitors in Microwave Frequency for NLTL Applications,” Proc. of the Fourth Workshop on Engineering and Space Technology (2013 WETE), S.J. Campos, SP, Aug. 2013.

14) J.O. Rossi, L.P. Silva Neto, and F.S. Yamasaki, “Key Issues in Design of NLTLs,” Proc. of the 41st IEEE International Conference on Plasma Science/Beams, Washington, DC, USA, May 2014, pp. 1-6.

15) J.O. Rossi , L.P. Silva Neto, and F.S. Yamasaki, “Operation of dielectric nonlinear transmission lines based on ceramic PZT slabs,” to be published in the Proc. of 2014 IEEE International Power Modulator and High Voltage Conference, Santa Fe, June 2014.

16) L.P. Silva Neto, J.O. Rossi, and J.J. Barroso, “Characterization of multilayer ferroelectric ceramic capacitors in a wide frequency range for RF applications,” Adv. Mat. Res., vol. 975, p. 61-66, July 2014.

17) L.P. Silva Neto and J.O. Rossi, “PZT dielectric ceramic characterization for application in nonlinear transmission lines,” Adv. Mat. Res., vol. 975, p.23-28, July 2014.

18) L.P. Silva Neto, J.O. Rossi, “PZT dielectric ceramic characterization for application in nonlinear transmission lines,” Advanced Materials Research, vol. 975, p.23-28, July 2014.

19) L.P. Silva Neto, J.O. Rossi, J.J. Barroso, and F.S. Yamasaki, “RF pulse formation in NLTLs using varactor diode,” Proc. of the Symposium of Operational Applications in Areas of Defense (SIGE), DCTA, S.J. Campos, SP, Sept. 2014, pp. 43-48.

20) A. R. Silva Jr., J.O. Rossi, L.P. Silva Neto, and M. Ueda, “Adherence Enhancement of Metallic Film on PZT-Type Ceramic Using Nitrogen Plasma Implantation. IEEE Transactions on Plasma Science. v.42, no. 10, pp.3173-3179, Oct. 2014.

21) L.P. Silva Neto, J.O. Rossi, J.J. Barroso, and A.R. Silva. “Characterization of Ceramic Dielectrics for Sub-GHz Applications in Nonlinear Transmission Lines”, IEEE Transactions on Plasma Science, v. 42, no. 10, p. 3274-3282, Oct. 2014.

22) F.S. Yamasaki, L.P. Silva Neto, J.O. Rossi, and J.J. Barroso “Soliton Generation Using Nonlinear Transmission Lines, IEEE Transactions on Plasma Science, v. 43, no. 11, pp. 3471- 3477, Nov. 2014.

23) P.A.D. Grilo, “Electromagnetic Magnetic Properties Characterization of Dielectric and Magnetic Substrates at High Frequency,” M.Sc. thesis, INPE, São José dos Campos, SP, Brazil, Dec. 2014 (in Portuguese).

24) L.P. Silva Neto, J.O. Rossi, P.A.G. Dias, and J.J. Barroso, “Frequency Characterization of Ferrite Beads in the Microwave Range for Nonlinear Applications,” Materials Science Forum, v.802, pp.552 - 557, Dec. 2014.

Collaborations on the Subject Supported by this Grant

- Prof. Edl Schamiloglu- University of New Mexico (UNM) – Dept. of Electrical and Computer Engineering- Head of the Pulsed Power, Beams and Microwaves Laboratory
- Dr. Ngee Siang Kuek –Dept. of Electrical and Computer Eng.– National University of Singapore (NUS)

Main Interactions

a. Participation in Conferences/Lectures/Workshops

- IEEE 2012 Int. Power Modulator and High Voltage Conference (IPMHVC), San Diego, CA, May 2012.
- IEEE/SBMO International Microwave and Electronics Conference (2013 IMOC), Rio Janeiro, RJ, Aug. 2013.
- IEEE 19th International Pulsed Power Conference (2013 PPC), San Francisco, CA, June 2013.
- The Ninth Int. Latin Conference on Power Technology (PTECH 2013), Campos do Jordão, Brazil, Oct. 2013.
- IEEE 2014 International Conference on Plasma Science (ICOPS) and Beams, Washington, DC, May 2014.
- IEEE 2014 Int. Power Modulator and High Voltage Conference (IPMHVC), Santa Fe, NM, June 2014.
- Fourth Workshop on Eng. and Space Technology, INPE, S. J. Campos, SP, Brazil, Aug. 2014.
- XVI Symposium of Operational Applications in Areas of Defense, ITA, S.J. Campos, SP, Brazil, Sept. 2014.

b. Technical Visits supported by this grant

- Prof. Edl Schamiloglu, Associated Plasma Laboratory, INPE, S.J. Campos, SP, Brazil, Feb. 2014
- Dr. Jose O. Rossi, ECE Dept., University of New Mexico, Albuquerque, NM, USA, May 2014.

Personnel Supported by this Grant

- Lauro P. Silva Neto – as D.Phil. Student
- Fernanda S. Yamasaky- as D.Phil. Student
- Ataide R. Silva – as D.Phil. Student
- Patricia A.G. Dias – as M.Sc. Student

1.

1. Report Type

Final Report

Primary Contact E-mail
Contact email if there is a problem with the report.

rossi@plasma.inpe.br

Primary Contact Phone Number
Contact phone number if there is a problem with the report

+551232086695

Organization / Institution name

INPE

Grant/Contract Title
The full title of the funded effort.

Study of HV Dielectrics for High Frequency Operation in Linear and Nonlinear Transmission Lines and Simulation and Development of Hybrid Nonlinear Lines for RF Generation

Grant/Contract Number
AFOSR assigned control number. It must begin with "FA9550" or "F49620" or "FA2386".

FA9550-13-1-0132

Principal Investigator Name
The full name of the principal investigator on the grant or contract.

Jose Osvaldo Rossi

Program Manager
The AFOSR Program Manager currently assigned to the award

James Fillerup

Reporting Period Start Date

03/01/2013

Reporting Period End Date

08/31/2014

Abstract

The objectives of this work is to describe the research on lumped capacitive nonlinear transmission lines (NLTLs) developed during period 2013-2014. As lumped capacitive NLTLs employ nonlinear dielectric mediums, we have characterized ceramic dielectrics (lead-zirconium and barium titanates, PZT and BT, respectively) in order to address RF soliton generation using these lines. Other issue studied was the investigation of the NLTL principle operation using a low voltage line built with varying capacitance diodes, called varactors, as these components show higher nonlinearity than commercial ceramic capacitors. To assess the performance of BT and PZT dielectrics we have built and tested HV NLTLs. In this case, the main results obtained and their implications on the design of capacitive NLTL operation at high frequencies are also discussed.

Distribution Statement
This is block 12 on the SF298 form.

Distribution A - Approved for Public Release

Explanation for Distribution Statement
If this is not approved for public release, please provide a short explanation. E.g., contains proprietary information.

SF298 Form

Please attach your SF298 form. A blank SF298 can be found here. Please do not password protect or secure the PDF The maximum file size for an SF298 is 50MB.

SF298-form.pdf

Upload the Report Document. File must be a PDF. Please do not password protect or secure the PDF . The maximum file size for the Report Document is 50MB.

Final Report- FA9550-13-1-0132.pdf

Upload a Report Document, if any. The maximum file size for the Report Document is 50MB.

Archival Publications (published) during reporting period:

1) L.P. Silva Neto, J.O. Rossi, and A.R. Silva, “Applications of PZT dielectric ceramics in high-energy storage systems,” Materials Science Forum, v. 727-728, pp. 505-510, 2012.
2) J.O. Rossi, L.P. Silva Neto, F.S. Yamasaki, and E. Schamiloglu, “Prospects of building capacitive nonlinear lines using ceramic PZT for high-frequency operation. Proc. of the 2012 IEEE International Power Modulator and High Voltage Conference (IPMHVC), San Diego, May 2012, p.752 -755.
3) N.S. Kuek, A.C. Liew, E. Schamiloglu, and J.O. Rossi, “Oscillating pulse generator based on a nonlinear inductive line,” IEEE Trans. Pla. Sci., v. 41, p. 2619-2624, 2013.
4) N.S. Kuek, A.C. Liew, E. Schamiloglu, and J.O. Rossi, “Pulsed RF oscillations on a nonlinear capacitive transmission line,” IEEE Trans. Diel. Elec. Ins., v. 20, pp. 1129-1135, Aug. 2013.
5) F.S. Yamasaki, “RF generation for aerospace applications using nonlinear transmission lines,” M.Sc. thesis, INPE, São José dos Campos, SP, Brazil, Feb. 2013 (in Portuguese).
6) A.R. Silva, J.O. Rossi, M. Ueda, and L.P.S. Neto, “Adherence Enhancement of Metallic Film on PZT Type Ceramic Using Nitrogen Plasma Implantation,” Proc. of the 19th IEEE International Pulsed Power Conference, San Francisco, CA. June 2013, pp. 1-4.
7) J.O. Rossi, L.P.S. Neto, and R.H.M. Siqueira, “Study of the Ceramic Capacitor Dielectric for Pulsed Power,” Proc. of the IEEE 19th International Pulsed Power Conference, San Francisco, CA, June 2013, pp. 1-4.
8) N.S. Kuek, A.C. Liew, E. Schamiloglu,and J.O. Rossi, “Generating RF pulses using a nonlinear hybrid line,” Proc. of the IEEE 19th International Pulsed Power Conference, San Francisco, CA, June 2013. pp. 1-5.
9) J.O. Rossi, E. Schamiloglu, N.S. Kuek, and F.S. Yamasaki, “Design considerations in lossy dielectric nonlinear transmission lines,” Proc. of the IEEE 19th International Pulsed Power Conference, San Francisco, CA, June 2013, pp. 1-5.
10) J.O. Rossi, L.P. Silva Neto, F.S. Yamasaki, and J.J. Barroso, “State of the art of nonlinear transmission lines for applications in high power microwaves,” Proc. of the SBMO/IEEE MTT-S International Microwave and Optoelectronics Conference, Rio de Janeiro, Brazil, Aug. 2013, pp. 1-5.
11) L.P. Silva Neto, J.O. Rossi, J.J. Barroso, A.R. Silva, P.J. Castro, and P.A.G. Dias, “Characterization of ceramic dielectrics for sub-GHz applications in nonlinear transmission lines,” Proc. of the SBMO/IEEE MTT-S International Microwave and Optoelectronics Conference, Rio de Janeiro, Brazil, Aug. 2013, pp. 1-5.
12) F.S. Yamasaki, J.O. Rossi, and J.J. Barroso, “Study of nonlinear lumped element transmission Lines for RF generation,” Proc. of the Fourth Workshop on Engineering and Space Technology (2013 WETE), S.J Campos, SP, Brazil, Aug. 2013.
13) L.P. Silva Neto, P.A.G. Dias, J.O. Rossi, and J.J. Barroso, “Characterization of Radial and Ceramic Capacitors in Microwave Frequency for NLTL Applications,” Proc. of the Fourth Workshop on Engineering and Space Technology (2013 WETE), S.J. Campos, SP, Aug. 2013.
14) J.O. Rossi, L.P. Silva Neto, and F.S. Yamasaki, “Key Issues in Design of NLTLs,” Proc. of the 41st IEEE International Conference on Plasma Science/Beams, Washington, DC, USA, May 2014, pp. 1-6.
15) J.O. Rossi , L.P. Silva Neto, and F.S. Yamasaki, “Operation of dielectric nonlinear transmission lines based on ceramic PZT slabs,” to be published in the Proc. of 2014 IEEE International Power Modulator and High Voltage Conference, Santa Fe, June 2014.
16) L.P. Silva Neto, J.O. Rossi, and J.J. Barroso, “Characterization of multilayer ferroelectric ceramic capacitors in a wide frequency range for RF applications,” Adv. Mat. Res., vol. 975, p. 61-66, July 2014.

17) L.P. Silva Neto and J.O. Rossi, “PZT dielectric ceramic characterization for application in nonlinear transmission lines,” Adv. Mat. Res., vol. 975, p.23-28, July 2014.
18) L.P. Silva Neto, J.O. Rossi, “PZT dielectric ceramic characterization for application in nonlinear transmission lines,” Advanced Materials Research, vol. 975, p.23-28, July 2014.
19) L.P. Silva Neto, J.O. Rossi, J.J. Barroso, and F.S. Yamasaki, “RF pulse formation in NLTLs using varactor diode,” Proc. of the Symposium of Operational Applications in Areas of Defense (SIGE), DCTA, S.J. Campos, SP, Sept. 2014, pp. 43-48.
20) A. R. Silva Jr., J.O. Rossi, L.P. Silva Neto, and M. Ueda, “Adherence Enhancement of Metallic Film on PZT-Type Ceramic Using Nitrogen Plasma Implantation. IEEE Transactions on Plasma Science. v.42, no. 10, pp.3173-3179, Oct. 2014.
21) L.P. Silva Neto, J.O. Rossi, J.J. Barroso, and A.R. Silva. “Characterization of Ceramic Dielectrics for Sub-GHz Applications in Nonlinear Transmission Lines”, IEEE Transactions on Plasma Science, v. 42, no. 10, p. 3274-3282, Oct. 2014.
22) F.S. Yamasaki, L.P. Silva Neto, J.O. Rossi, and J.J. Barroso “Soliton Generation Using Nonlinear Transmission Lines, IEEE Transactions on Plasma Science, v. 43, no. 11, pp. 3471- 3477, Nov. 2014.
23) P.A.D. Grilo, “Electromagnetic Magnetic Properties Characterization of Dielectric and Magnetic Substrates at High Frequency,” M.Sc. thesis, INPE, São José dos Campos, SP, Brazil, Dec. 2014 (in Portuguese).
24) L.P. Silva Neto, J.O. Rossi, P.A.G. Dias, and J.J. Barroso, “Frequency Characterization of Ferrite Beads in the Microwave Range for Nonlinear Applications,” Materials Science Forum, v.802, pp.552 - 557, Dec. 2014.

Changes in research objectives (if any):

Change in AFOSR Program Manager, if any:

Extensions granted or milestones slipped, if any:

AFOSR LRIR Number

LRIR Title

Reporting Period

Laboratory Task Manager

Program Officer

Research Objectives

Technical Summary

Funding Summary by Cost Category (by FY, $K)

	Starting FY	FY+1	FY+2
Salary			
Equipment/Facilities			
Supplies			
Total			

Report Document

Report Document - Text Analysis

Report Document - Text Analysis

Appendix Documents

2. Thank You

E-mail user

Aug 25, 2015 14:51:47 Success: Email Sent to: rossi@plasma.inpe.br